

RESEARCH

Open Access



Neuronal TDP-43 aggregation drives changes in microglial morphology prior to immunophenotype in amyotrophic lateral sclerosis

Molly E. V. Swanson^{1,2}, Miran Mrkela^{1,2}, Clinton Turner³, Maurice A. Curtis^{2,4}, Richard L. M. Faull^{2,4}, Adam K. Walker⁵ and Emma L. Scotter^{1,2*}

Abstract

Microglia are the innate immune cells of the brain with the capacity to react to damage or disease. Microglial reactions can be characterised in post-mortem tissues by assessing their pattern of protein expression, or immunophenotypes, and cell morphologies. We recently demonstrated that microglia have a phagocytic immunophenotype in early-stage ALS but transition to a dysfunctional immunophenotype by end stage, and that these states are driven by TAR DNA-binding protein 43 (TDP-43) aggregation in the human brain. However, it remains unclear how microglial morphologies are changed in ALS. Here we examine the relationship between microglial immunophenotypes and morphologies, and TDP-43 pathology in motor cortex tissue from people with ALS and from a TDP-43-driven ALS mouse model. Post-mortem human brain tissue from 10 control and 10 ALS cases was analysed alongside brain tissue from the bigenic *NEFH-tTA/tetO-hTDP-43ΔNLS* (rNLS) mouse model of ALS at distinct disease stages. Sections were immunohistochemically labelled for microglial markers (HLA-DR, CD68, and Iba1) and phosphorylated TDP-43 (pTDP-43). Single-cell microglial HLA-DR, CD68, and Iba1 average intensities, and morphological features (cell body area, process number, total outgrowth, and branch number) were measured using custom image analysis pipelines. In human ALS motor cortex, we identified a significant change in microglial morphologies from ramified to hypertrophic, which was associated with increased Iba1 and CD68 levels. In the rNLS mouse motor cortex, the microglial morphologies changed from ramified to hypertrophic and increased Iba1 levels occurred in parallel with pTDP-43 aggregation, prior to increases in CD68 levels. Overall, the evidence presented in this study demonstrates that microglia change their morphologies prior to immunophenotype changes. These morphological changes may prime microglia near neurons with pTDP-43 aggregation for phagocytosis, in turn triggering immunophenotype changes; first, to a phagocytic state then to a dysfunctional one.

Keywords Amyotrophic lateral sclerosis, Microglia, TDP-43, Iba1, CD68, Ramified, Hypertrophic, Dystrophic

*Correspondence:
Emma L. Scotter
emma.scotter@auckland.ac.nz

Full list of author information is available at the end of the article



© The Author(s) 2025. **Open Access** This article is licensed under a Creative Commons Attribution 4.0 International License, which permits use, sharing, adaptation, distribution and reproduction in any medium or format, as long as you give appropriate credit to the original author(s) and the source, provide a link to the Creative Commons licence, and indicate if changes were made. The images or other third party material in this article are included in the article's Creative Commons licence, unless indicated otherwise in a credit line to the material. If material is not included in the article's Creative Commons licence and your intended use is not permitted by statutory regulation or exceeds the permitted use, you will need to obtain permission directly from the copyright holder. To view a copy of this licence, visit <http://creativecommons.org/licenses/by/4.0/>.

Introduction

Microglia are the innate immune cells of the brain, with functional roles in both health and disease. Microglia have the capacity to respond to damage and disease, performing functions such as phagocytosis, cytokine secretion, migration, and antigen presentation [1–13]. To fulfil and switch between these functions, microglia change their morphologies and protein expression, and such changes have been identified in a range of neurodegenerative diseases including amyotrophic lateral sclerosis (ALS) [14–30]. However, while these microglial changes are likely neuroprotective in early-stage ALS, there is evidence that microglia become dysfunctional and neurotoxic in late-stage disease [31–33].

ALS is the most common form of motor neuron disease, characterised by progressive death of upper and lower motor neurons, which leads to muscle atrophy, disability, and death [34]. Diverse genetic and environmental factors cause or increase the risk of ALS [35, 36]. Despite this range of risk factors, 97% of all ALS cases share a common pathological hallmark: intracellular accumulation of TAR DNA-binding protein 43 (TDP-43) aggregates in motor neurons [37]. Although TDP-43 aggregates are unlikely to be the ‘toxic species’ in ALS, they are surrogates for the presence of the aggregation pathway species that *are* thought to be toxic; misfolded monomers and oligomers [38]. While motor neurons are central to ALS pathogenesis and symptomatology, microglial immunophenotypes (pattern of protein expression) and morphologies are also altered in response to TDP-43 aggregation [20, 32, 39–41]. Indeed, in the human ALS brain, microglia up-regulate markers suggestive of increased phagocytosis and dysfunction [39]. However, there has been limited consideration of microglial morphology changes in conjunction with immunophenotypes in the ALS brain.

Microglial morphologies have been examined in post-mortem studies to infer function and/or dysfunction in the ageing and diseased brain [42–51]. Five distinct morphologies have been described: ramified (small cell bodies and complex processes), hypertrophic (large cell bodies with reduced process complexity), dystrophic (small cell bodies with beaded, discontinuous, or tortuous processes), amoeboid (round cell body with pseudopodia), and rod (elongated appearance with small cell body and retraction of planar processes) [42–44, 46, 50, 52–57]. While analyses of microglial morphology in ALS are limited, immunohistochemical labelling of a cytoskeletal protein expressed by all microglia, Iba1, has been used to identify morphological changes in rodent *SOD1* ALS models [15, 17, 18, 21]. Microglia in control mice and transgenic rodents at early disease stages have small cell bodies with complex processes, suggestive of a ramified ‘resting’ morphology. In contrast, microglia in

ALS transgenic mice at later disease stages have larger cell bodies with reduced process complexity, suggestive of a hypertrophic ‘reactive’ morphology [15, 17, 18, 21]. A recent study demonstrated that rod-shaped microglia may play a unique neuroprotective role in TDP-43 mice and human sporadic ALS; however, hypertrophic and dystrophic microglia classically identified in ALS brains were not described [41]. Further investigations into how microglial morphologies change in response to the neuronal TDP-43 aggregation characteristic of more than 97% of ALS cases and how these changes relate to function are needed.

While microglial morphology can be used to infer microglial functional states, microglial functions are not thought to be specific to a given morphology. Numerous microglia classification paradigms that consider microglial morphologies and immunophenotypes have been proposed to describe microglial responses in the human brain, including but not limited to; activated versus resting microglia, M1/M2 pro- and anti-inflammatory microglia, and disease-associated microglia (DAMs) [51]. However, these somewhat binary classifications of microglial states do not accurately describe microglial heterogeneity in human health or disease [51]. To this end, integrative methodological approaches that can deeply phenotype microglia at the single-cell level have been employed to characterise microglial changes in ageing and disease. In the context of ALS, single cell and bulk RNA sequencing has been used to identify microglial states and assess their changes in rodent models and ALS patients [20, 22, 28–30, 40, 58–61], but their validation at the protein level in the human ALS brain has been limited. We recently utilised multiplexed immunohistochemistry to identify microglial changes relative to TDP-43 pathology in ALS [39]. We demonstrated that microglia have a phagocytic immunophenotype at early-stage ALS but transition to a dysfunctional immunophenotype at end-stage disease, and that these immunophenotypes are driven by TDP-43 aggregation [39], validating previous microglial states identified by RNA sequencing [40]. It is currently unclear how microglial morphologies change with respect to protein expression changes, but highly multiplexed immunohistochemistry enables the analysis of both concurrently, and the potential to infer changes in microglial function in the ALS brain.

This study aims to explore both microglial immunophenotype and morphology to characterise microglial states in ALS. We use automated single-cell protein expression and morphological analyses of immunohistochemically labelled tissue to compare changes in microglial immunophenotype and morphology in ALS brains and age-matched normal controls. We also infer temporal changes in microglial immunophenotype and

morphology in ALS by examining TDP-43 mouse model brain tissue at disease onset, early disease, and late disease stages [62]. Our data demonstrate that microglia alter their morphologies parallel to pTDP-43 aggregation in ALS and that these alterations precede changes in levels of the microglial proteins HLA-DR, CD68, and Iba1. The immunophenotype and morphology data we present in this study support the hypothesis that microglial morphological alterations occur early in the ALS brain.

Materials and methods

Human case selection

Formalin-fixed paraffin-embedded motor cortex blocks from 10 neurologically normal and 10 ALS cases from the Neurological Foundation Human Brain Bank (HuBB) at the Centre for Brain Research, University of Auckland were used in this study (Table 1). This cohort of cases was examined as part of a previous study [39], but new tissue sections, immunolabelling, imaging, and analyses were performed here. Control cases had no previous history of neurological disorders and cause of death was unrelated to any neurological condition. ALS cases were diagnosed clinically by consultant neurologists at Auckland City or Middlemore Hospitals (Auckland, New Zealand) during life. All case classifications were confirmed with post-mortem neuropathology assessments performed by consultant neuropathologists at Auckland City Hospital. All ALS cases showed pTDP-43 deposition in the motor cortex. ALS cases were further classified as stage 1–3 or

stage 4 pTDP-43 pathology based on the absence or presence of pTDP-43 aggregates in the hippocampus, respectively [63].

The fixation and dissection of anatomical regions from human brains by the HuBB has been described previously [64]. Briefly, human brains were obtained at autopsy and the right hemisphere was fixed by perfusion of 15% formaldehyde in 0.1 M phosphate buffer through the cerebral arteries. Brains were subsequently dissected into approximately 60 regional blocks and 1-cm thick blocks from each region were processed for paraffin embedding. For this study, 10- μ m thick sections were cut from paraffin-embedded motor cortex blocks from all control and ALS cases (Table 1) using a rotary microtome and mounted on ÜberFrost® Printer Slides (InstrumeC).

Mouse tissue collection

rNLS double-transgenic experimental mice and monogenic litter-mate controls were produced from crosses of hemizygous B6.C3-Tg(NEFH-tTA)8Vle/JAusb mice (NEFH-tTA line 8, stock #025,397) with homozygous B6.C3-Tg(*tetO-TARDBP**)4Vle/JAusb mice (*tetO-hTDP-43^{ΔNLS}* line 4, stock #014,650), originally obtained from Jackson Laboratories [62] following backcrossing of each independent line for >10 generations on C56BL/6JAusb (Australian BioResources) background. Intercross mice and offspring were provided with 200 mg/kg doxycycline (Dox)-containing feed (Specialty Feeds, Australia) until 8–12 weeks of age. Both sexes were included

Table 1 Post-mortem case demographics

Group	Case code	Age (y)	Sex	PMD (h)	fALS/sALS	
Neurologically Normal Controls (n = 10)	H211	41	M	8	-	
	H215	67	F	23.5	-	
	H226	73	F	48	-	
	H230	57	F	32	-	
	H238	63	F	16	-	
	H240	73	M	26.5	-	
	H242	61	M	19.5	-	
	H245	63	M	20	-	
	H247	51	M	31	-	
	H249	77	F	17	-	
Control mean \pm SD	-	62.60 \pm 10.95	5 M:5 F	24.15 \pm 11.06	-	
ALS (n = 10)	Stage 1–3 (n = 5)	MN11	77	F	18	fALS (unknown)
		MN14	59	F	19	fALS (unknown)
		MN16	69	M	16.5	sALS
		MN20	85	M	15	sALS
		MN25	71	M	23.5	sALS
	Stage 4 (n = 5)	MN13	55	M	10	sALS (ANXA11 p.G38R)
		MN15	54	F	18	sALS
		MN19	75	M	20.5	sALS
		MN29	72	M	24	sALS
		MN30	84	F	17.5	sALS
ALS mean \pm SD	-	70.10 \pm 11.07	6 M:4 F	18.20 \pm 4.063	-	

in each group, and mice were housed under 12 h light/dark cycle at 21 ± 1 °C and $55 \pm 5\%$ humidity. Brains were collected from mice as described previously [65]. Animal ethics approval was obtained from The University of Queensland (#QBI/131/18), and experiments were conducted in accordance with the Australian code of practice for the care and use of animals for scientific purposes.

Multiplexed fluorescence immunohistochemistry and imaging of human ALS brain

A 5-plex immunohistochemistry labelling panel was designed to quantify microglial immunophenotypes (anti-CD68, -HLA-DR, and -Iba1) and morphology (anti-Iba1) relative to pathology (pTDP-43) per cell (Hoechst nuclear stain) (Table 2, quantification panel). CD68 and Iba1 were subsequently co-labelled to validate their expression by microglia with specific morphologies (Table 2, confocal panel).

Immunohistochemical labelling of paraffin-embedded motor cortex sections was carried out as previously described [39, 66, 67]. Briefly, Tris-EDTA pH 9.0 antigen retrieval was performed, and sections were incubated in primary then secondary antibody mixtures (Table 2). Sections were washed thoroughly in phosphate-buffered

saline between each step. Nuclei were counterstained with Hoechst 33,258 and sections were coverslipped using ProLong® Gold Antifade mounting media.

Sections labelled with the 5-plex immunohistochemical panel were imaged on a Zeiss Z2 Axioimager (20×/0.9 NA) using MetaSystems VSlide acquisition software and MetaCyte stitching software. The Zeiss Z2 Axioimager used a Colibri 7 solid-state light source with LED lamps and the following filter sets to enable spectral separation of the 5 fluorophores per round (Ex peak (nm); Em peak (nm)/bandpass (nm)): Hoechst 33,258 (385; 447/60), AlexaFluor® 488 (475; 550/32), AlexaFluor® 546 (555; 580/23), AlexaFluor® 594 (590; 628/32), and AlexaFluor® 647 (630; 676/29).

Sections labelled with anti-CD68 and -Iba1 only were imaged on a Zeiss LSM 800 Airyscan confocal microscope (63×/1.4 NA, oil immersion) using ZEN 2.6 software (Zeiss). Optical z-stacks were taken through the entirety of the cell body and processes. Images were acquired using the built-in Airyscan module and processed using the ZEN microscopy software (Zeiss). Maximum intensity z-projections were generated and processed using FIJI (v 1.53 C).

Multiplexed fluorescence immunohistochemistry and imaging of transgenic mouse model ALS brain

Brain tissue from a bigenic *NEFH-tTA/tetO-hTDP-43ΔNLS* (rNLS) mouse model of ALS (and litter-matched controls) at disease onset, early disease, and late disease stages (2, 4, and 6 weeks off doxycycline (WOD), respectively) was immunohistochemically labelled with CD68, Iba1, NeuN, and pTDP-43 and imaged on a Zeiss Z2 Axioimager (20×/0.9 NA) using MetaSystems VSlide acquisition software and MetaCyte stitching software (as described above) [39]. The images from this cohort of rNLS mice were generated and analysed as part of a previous study [39], but new analyses were performed on these images here and new data presented.

Quantification of microglial features and ALS pathology using MetaMorph image analysis pipelines

To quantify microglial protein expression levels and morphological features in the human and transgenic mouse model ALS brain, custom image analysis pipelines were developed in Metamorph software (Molecular Devices), similar to those previously described [39, 68, 69]. Prior to all analyses, manual regions of interest (ROI) were drawn on each Hoechst image to isolate cortical layers I-VI for analysis and exclude tissue folds and defects.

Tissue-wide microglial and pTDP-43 integrated intensity analyses

To identify global microglial and pTDP-43 changes in the ALS motor cortex, the tissue-wide abundance of

Table 2 Immunohistochemistry panels for analysis of microglia changes in the human ALS brain

PANEL 1 Quantification panel			
Primary antibody, Concentration	Company, Catalogue number	Secondary antibody, Concentration	Company, Catalogue number
Rabbit IgG anti-pTDP-43 (Ser 409/410), 1:3,000	Cosmobio, TIP-PTD-P02	Goat anti-rabbit AlexaFluor® 488, 1:500	Jackson Laboratories, 111-545-144
Mouse IgG ₁ anti-HLA-DR, 1:1,000	DAKO, M0775	Goat anti-mouse IgG1 AlexaFluor® 546, 1:500	Thermo Fisher Scientific, A21123
Mouse IgG ₃ anti-CD68, 1:200	Abcam, ab783	Goat anti-mouse IgG3 AlexaFluor® 594, 1:500	Thermo Fisher Scientific, A21155
Guinea pig IgG anti-Iba1, 1:2,000	Synaptic Systems, 234-004	Goat anti-chicken AlexaFluor® 647, 1:500	Thermo Fisher Scientific, A21450
PANEL 2 Confocal panel			
Primary antibody, Concentration	Company, Catalogue number	Secondary antibody, Concentration	Company, Catalogue number
Chicken IgY anti-Iba1, 1:1,000	Synaptic Systems, 234-009	Goat anti-chicken AlexaFluor® 488, 1:500	Thermo Fisher Scientific, A11039
Rabbit IgG anti-CD68, 1:1,000	Abcam, ab215212	Goat anti-rabbit AlexaFluor® 594, 1:500	Jackson Laboratories, 115-585-166

each microglial marker and pTDP-43 was measured. For the human tissue, binary masks of CD68, HLA-DR, and Iba1 immunolabelling were generated using the adaptive thresholding tool. These three binary masks were combined to create a master mask, encompassing all microglia immunoreactive for CD68, HLA-DR, and/or Iba1. For the mouse tissue, a binary mask of only Iba1 was generated to identify all microglia as all microglia were highly immunoreactive for Iba1. The integrated intensity of each marker was measured across the master mask (human) or Iba1 mask (mouse) and normalised to the ROI area to give a measure of tissue-wide expression. To measure the tissue-wide abundance of pTDP-43, a binary mask of specific pTDP-43 immunoreactivity was generated using the threshold clip tool. The integrated intensity of pTDP-43 labelling within this binary mask was measured and normalised to ROI area.

Tissue-wide microglial morphology analyses

To identify overall microglial morphology changes in the ALS motor cortex, the tissue-wide averages of key cell morphology features were measured: cell body area, process number, total outgrowth, and branch number. These cell morphology features were measured from the Iba1 image using the Metamorph in-built Neurite Outgrowth application. This application identified microglial cell bodies based on manually determined maximum cell body width, cell body Iba1 intensity above local background, and minimum cell body area, and microglial processes based on maximum process width, process Iba1 intensity above local background, and minimum process length to be considered significant.

Single-cell microglial immunophenotype and morphology analyses

Next, all microglia within each ROI were identified and the single-cell expression of CD68, HLA-DR, and Iba1 and cell morphology was measured. Using the microglial master mask generated for the tissue-wide microglial integrated intensity analysis, the watershed lines morphology filter was used to identify the border of each microglial domain; each microglia and its domain was contained within its own border. To quantify the single-cell expression of each microglial marker, the average intensity of CD68, HLA-DR, and Iba1 within the master mask was measured in each microglial domain. To quantify the single-cell morphology features, cell body area, process number, total outgrowth, and branch number were measured from Iba1 using the Neurite Outgrowth application in each microglial domain.

Microglial phenotype and morphological feature clustering

To identify potential clusters of microglial immunophenotypes or morphologies, cells were evenly sampled across the different groups. For the human data, 7,340 cells each were randomly sub-sampled from stage 1–3 ALS, stage 4 ALS, and normal cases for a total of 22,020 cells. The single-cell morphological features of mean microglial cell body area, process number, total outgrowth, and branch number in addition to mean cell intensities of Iba1 and CD68 were included in our dataset. These were log-transformed for equal weighting and a k-nearest neighbor (KNN) graph was constructed with the k parameter set as $\sqrt{N_{cells}}$. For the cell clustering, a community detection clustering approach (Louvain clustering) was applied with the resolution (clustering granularity) set to 1.0 wherein a total of 11 cluster assignments were obtained. All data processing and subsequent clustering was conducted in R v.4.2 using the 'FNN v.1.1.3' and 'igraph v.1.2.11' packages [70, 71].

Statistical analyses

For human analyses, pTDP-43 and microglial marker tissue-wide integrated intensities and microglial morphology measures were compared between case groups with multiple Mann-Whitney tests and multiple comparisons were controlled for using a False Discovery Rate of 0.01, as determined by the two-stage step-up method of Benjamini, Krieger, and Yekutieli. Statistical significance was set at $p \leq 0.05$ with significances of difference between case groups shown as $*p \leq 0.05$, $**p \leq 0.01$, $***p \leq 0.001$, $****p \leq 0.0001$. pTDP-43 and microglial marker tissue-wide integrated intensities and microglial morphology measures were sequentially correlated with one another using Spearman correlations. When $r \leq -0.7$ or $r \geq 0.7$ and $p \leq 0.05$, correlations were considered statistically significant and strong. When $-0.7 < r \leq -0.4$ or $0.7 > r \geq 0.4$ and $p \leq 0.05$, correlations were considered statistically significant and moderate. For the microglial clustering analysis, the percentage of microglia in each cluster was compared between case groups using a 2-way ANOVA with Tukey's multiple comparisons test, and the mean single cell CD68 and Iba1 average intensities were compared between clusters using a Kruskal-Wallis test with Dunn's multiple comparisons test.

For mouse analyses, microglial intensity and morphology measures were compared between case groups at each time point with 2-way ANOVA with Tukey's multiple comparisons test. Statistical significance was set at $p \leq 0.05$ with the significance of differences between groups shown as $*p \leq 0.05$, $**p \leq 0.01$, $***p \leq 0.001$, $****p \leq 0.0001$.

Results

Increased microglial CD68 and Iba1 levels and pTDP-43 abundance in the human ALS motor cortex

Immunohistochemistry was used to identify microglial markers HLA-DR, CD68, and Iba1, and pTDP-43 aggregates, in the control and ALS motor cortex including cases previously shown to have pTDP-43 in defined regions including the hippocampus (representing more advanced disease, 'stage 4 ALS') [63] and cases with pTDP-43 in the motor cortex and/or spinal cord but not hippocampus (representing less advanced disease, 'stage 1–3 ALS'; Fig. 1A–E). Tissue-wide integrated intensity analyses revealed that microglial HLA-DR intensity remained unchanged in ALS (Fig. 1F), while CD68 and Iba1 intensities were significantly increased in both stage 1–3 ALS and stage 4 ALS compared with controls (Fig. 1G and H). As expected, we observed no pTDP-43 pathology in the motor cortex of control cases (Fig. 1B and I), with pTDP-43 only seen in ALS cases (Fig. 1C, E, and I). However, a statistically significant increase in pTDP-43 compared with controls was only seen in stage 4 ALS cases, likely due to the variability in pTDP-43 pathology levels in stage 1–3 cases (Fig. 1I).

Microglial morphologies change in human ALS and correlate with CD68 and Iba1 levels

We subsequently sought to identify whether microglial morphologies were altered in the human ALS motor cortex. Microglial cell bodies and processes were identified by Iba1 immunoreactivity using the Metamorph Neurite Outgrowth application (Fig. 2A), as previously described [72]. Single-cell morphology measurements of cell body area, process number, total outgrowth, and branch number were averaged across all microglial cells in each case to give a mean measure per microglia (Fig. 2B–E). We identified significant changes in microglial morphology measures in ALS: cell body area and process number were increased in stage 1–3 ALS compared with controls (Fig. 2B and C), and total outgrowth was significantly reduced in stage 4 ALS compared with controls (Fig. 2D).

To identify whether microglial morphological changes correlated with pTDP-43 pathology and/or microglial HLA-DR, CD68, and Iba1 levels, the mean morphology measures above were sequentially correlated with tissue-wide pTDP-43, HLA-DR, CD68, and Iba1, integrated intensities (Fig. 2F and S1). In accordance with the pattern of changes in the human ALS motor cortex (Fig. 1), pTDP-43, CD68, and Iba1 showed significant strong positive correlations with one another (Fig. 2F). pTDP-43, CD68, and Iba1 also all showed significant correlations with all morphology measures: moderate to strong positive correlations with cell body area and process number, and moderate negative correlations with total outgrowth and branch number. Furthermore,

morphological measures significantly correlated with one another (Fig. 2F and S1). This suggests that as microglial CD68 and Iba1 levels increase in ALS with increased pTDP-43 aggregation, microglia also reduce their outgrowth and branch number, and increase their process number and cell body area, suggestive of hypertrophic morphology.

Microglial clusters enriched in human ALS are characterised by high Iba1 and CD68 levels with hypertrophic and dystrophic morphologies

Having determined that microglial morphology and functional marker expression are altered in ALS and are correlated, we sought to identify specific microglial phenotypes emerging in ALS. To identify microglial phenotypes enriched in ALS cases, microglia from control, stage 1–3 ALS, and stage 4 ALS cases were clustered based on the single cell CD68, HLA-DR, and Iba1 average intensities, and morphological measures (cell body area, process number, total outgrowth, and branch number). A total of 11 unique clusters were identified, with 4 clusters (numbered arbitrarily) being differentially abundant in ALS compared with control cases (Fig. 3A). Clusters 1 and 8 were depleted in ALS cases: cluster 1 was significantly more abundant in control cases compared with stage 4 ALS cases, and cluster 8 was significantly more abundant in control cases compared with both stage 1–3 ALS and stage 4 ALS cases (Fig. 3A). However, no significant correlations between the abundance of control- or ALS-enriched clusters and pTDP-43 intensity were identified (Fig. 3B and C).

We subsequently phenotyped the ALS-depleted and ALS-enriched microglial clusters, characterising their CD68 and Iba1 levels and morphological characteristics (Fig. 3D–F). The ALS-enriched clusters 4 and 10 had significantly higher CD68 and Iba1 average intensities than the ALS-depleted clusters (Fig. 3D and E) or the clusters equally present in ALS and control cases (Fig. S2). Furthermore, ALS-enriched cluster 4 had significantly higher CD68 and Iba1 average intensities than ALS-enriched cluster 10 (Fig. 3D and E). ALS-depleted and ALS-enriched clusters also showed unique morphological characteristics. Only cell body area and branch number and were assessed because the mean cell body area showed a strong significant correlation with process number ($r=0.85$, $p<0.0001$), and branch number in each cluster showed a strong significant correlation with total outgrowth ($r=0.99$, $p<0.0001$). ALS-depleted clusters 1 and 8 had smaller cell bodies with high branch numbers, reminiscent of a ramified morphology (Fig. 3F and S3), implying depletion of ramified microglia in ALS. Conversely, ALS-enriched clusters had larger cell bodies with low branch numbers with reminiscent of hypertrophic and dystrophic morphologies (Fig. 3F and S3).

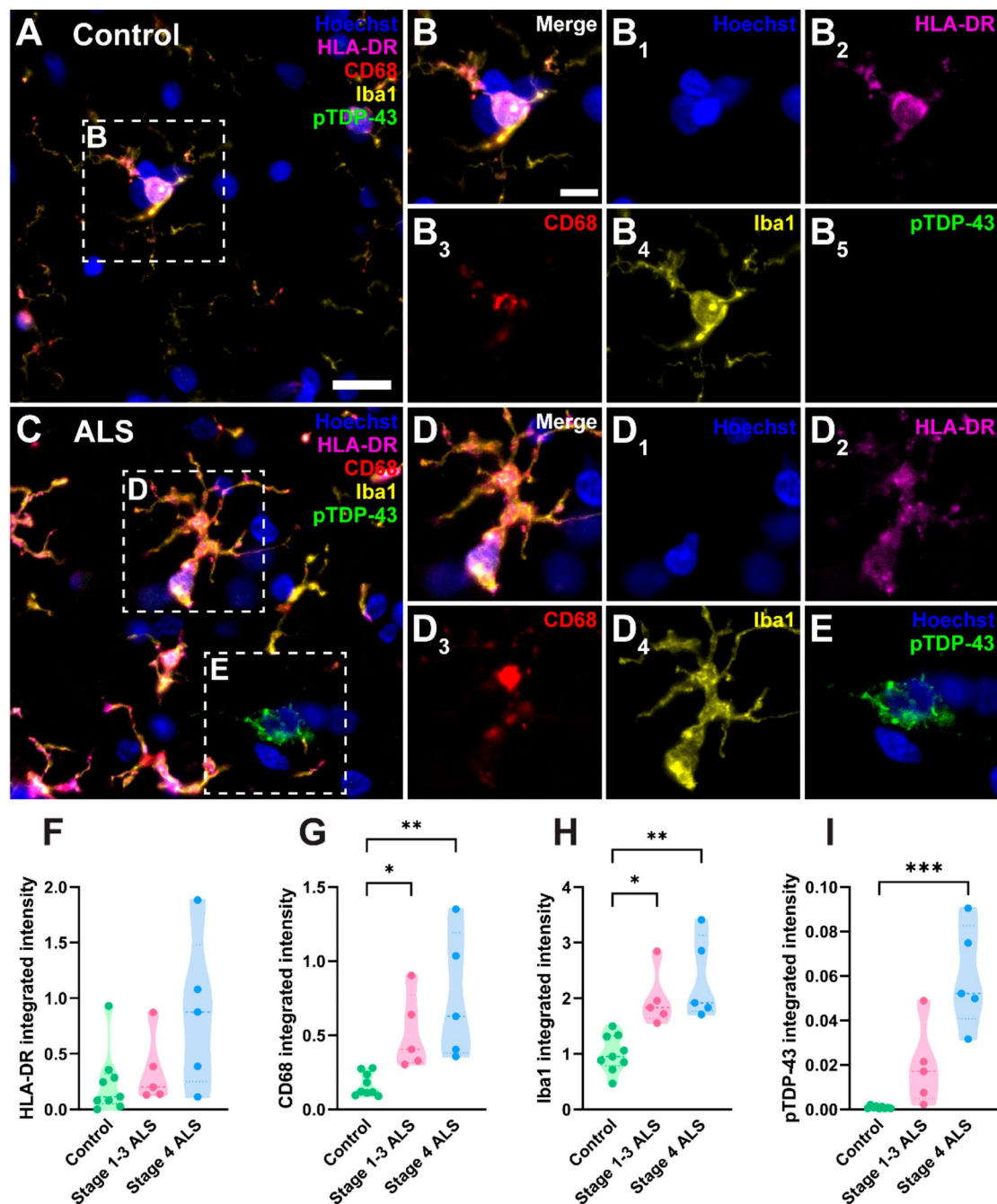


Fig. 1 Increased microglial CD68 and Iba1 levels and pTDP-43 abundance in the human ALS motor cortex. Immunohistochemical labelling was used to visualise microglia and pTDP-43 in the motor cortex from human control (A–B), stage 1–3 (not shown), and stage 4 ALS (C–E) cases. Microglial markers, HLA-DR (magenta), CD68 (red), and Iba1 (yellow), were co-labelled with pTDP-43 (green) and a Hoechst nuclear counterstain (blue). Scale bar (A and C) = 20 μm and scale bar (B, D, and E) = 10 μm. Total microglia were identified by creating separate binary masks from thresholded HLA-DR, CD68, and Iba1 images which were then combined to create a microglial master mask [39, 69, 86]. The total integrated intensities of HLA-DR (F), CD68 (G), and Iba1 (H) were measured within this master mask, normalised to tissue area and compared between control, stage 1–3 ALS, and stage 4 ALS cases. The total integrated intensity of pTDP-43 aggregates normalised to tissue area was quantified and compared between normal, stage 1–3 ALS, and stage 4 ALS cases (I). Data presented as truncated violin plots with median and quartiles shown; control $n = 10$, stage 1–3 ALS $n = 5$, and stage 4 ALS $n = 5$. All intensity measures were compared between case groups with multiple Mann-Whitney tests and multiple comparisons were controlled for using a False Discovery Rate of 0.01, as determined by the two-stage step-up method of Benjamini, Krieger, and Yekutieli. Significances of difference between case groups: * $p \leq 0.05$, ** $p \leq 0.01$, *** $p \leq 0.001$

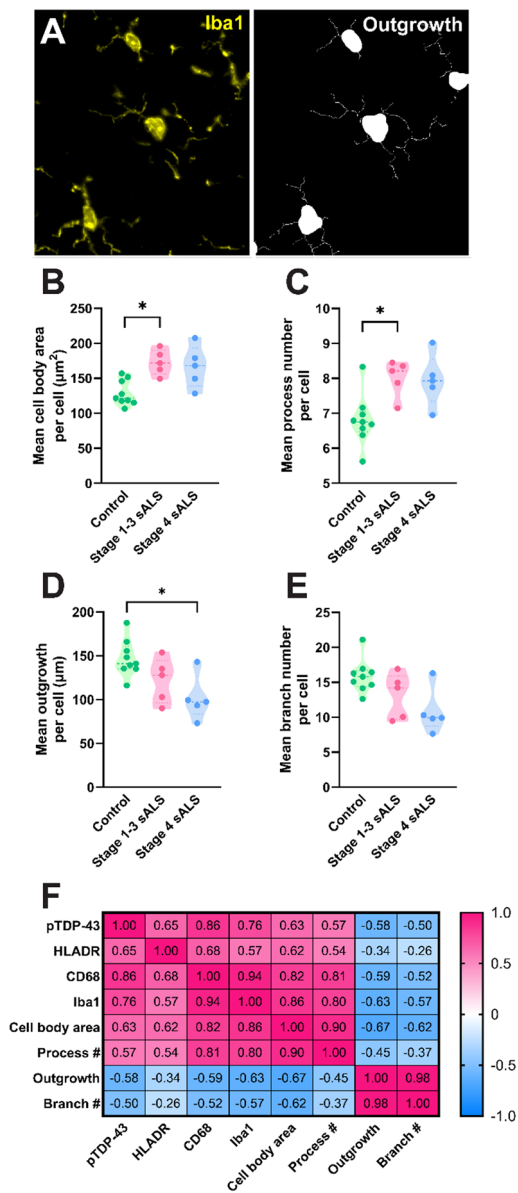


Fig. 2 Microglial morphologies change in human ALS and correlate with CD68 and Iba1 levels. Microglial cell bodies and processes were identified using Iba1 immunoreactivity (A, yellow) and used to quantify morphology measures per cell (A, white): cell body area (B), process number (C), outgrowth (D), and branch number (E). Single-cell measures were averaged across all microglia in each case to give a mean measure per cell which was compared between control, stage 1–3 ALS, and stage 4 ALS cases. Data presented as truncated violin plots with median and quartiles shown; control $n=10$, stage 1–3 ALS $n=5$, and stage 4 ALS $n=5$. All morphology measures were compared between case groups with multiple Mann-Whitney tests and multiple comparisons were controlled for using a False Discovery Rate of 0.01, as determined by the two-stage step-up method of Benjamini, Krieger, and Yekutieli. Significances of difference between case groups: $*p \leq 0.05$. Measures of pTDP-43 pathology, microglial marker intensities, and microglial morphology were sequentially correlated in all cases ($n=20$) using Spearman correlations (F). The resulting r value from each correlation is presented in the correlation matrix and colour coded relative to strength. When $r \leq -0.7$ or $r \geq 0.7$ and $p \leq 0.05$, correlations were considered statistically significant and strong. When $-0.7 < r \leq -0.4$ or $0.7 > r \geq 0.4$ and $p \leq 0.05$, correlations were considered statistically significant and moderate

We confirmed the presence of CD68^{low} Iba1^{low} ramified microglia (clusters 1 and 8) and CD68^{high} Iba1^{high} hypertrophic and dystrophic microglia (clusters 4 and 10) in the control and ALS motor cortex using confocal microscopy (stage 4 ALS case example images shown in Fig. 3G-I).

Microglial Iba1 and morphological changes occur parallel to pTDP-43 aggregation and prior to CD68 changes in the TDP-43-driven rNLS mouse model of ALS

With changes in microglial marker expression and morphological features, we sought to determine *when* these microglial changes occur with respect to the development of pTDP-43 aggregation. To understand this relationship temporally, we utilised brain tissue from bigenic *NEFH-tTA/tetO-hTDP-43ΔNLS* (rNLS) and single transgenic *tetO-hTDP-43ΔNLS* (control) mice at 2, 4, and 6 weeks off doxycycline (WOD), equivalent to disease onset, early disease, and late disease stages, respectively [62].

We first investigated the presence of ramified, hypertrophic, and dystrophic microglia in the rNLS mouse motor cortex. Indeed, as per the human ALS motor cortex, we identified all three microglial morphologies in the rNLS motor cortex at 6 WOD (Fig. 4A-C). Furthermore, hypertrophic and dystrophic microglia showed increased CD68 expression (Fig. 4B and C), as per human microglia clusters 4 and 10.

To quantify microglial morphological features relative to CD68 and Iba1 levels and neuronal pTDP-43 levels, we utilised images from a previous study [39] (Fig. 4D). Using these images, we have previously shown an increase in the percentage of CD68^{high} microglia at 4 WOD, occurring after the accumulation of pTDP-43 from 2 WOD (Fig. 4E). In the current study, we identified a significant increase in CD68 integrated intensity at 4 and 6 WOD in rNLS mice relative to controls (Fig. 4F). In addition, Iba1 integrated intensity was significantly increased from 2 WOD in the rNLS mouse cohort relative to controls (Fig. 4G), suggesting microglial changes occur prior to the CD68 changes observed at 4 WOD.

Changes in microglial morphological measures were also identified from 2 WOD in the rNLS mice (Fig. 4H-K). At 2 WOD, rNLS mouse microglia had unchanged cell body area and process number, but significantly reduced total outgrowth and branch number, suggesting a change towards a hypertrophic morphology (Fig. 4H-K). At 4 WOD, rNLS mouse microglia had significantly increased cell body area and process number and significantly reduced total outgrowth and branch number, suggesting predominantly hypertrophic morphologies (Fig. 4H-K). Finally, at 6 WOD, rNLS mouse microglia resembled 2 WOD microglia, with unchanged cell body area and process number, and significantly reduced total

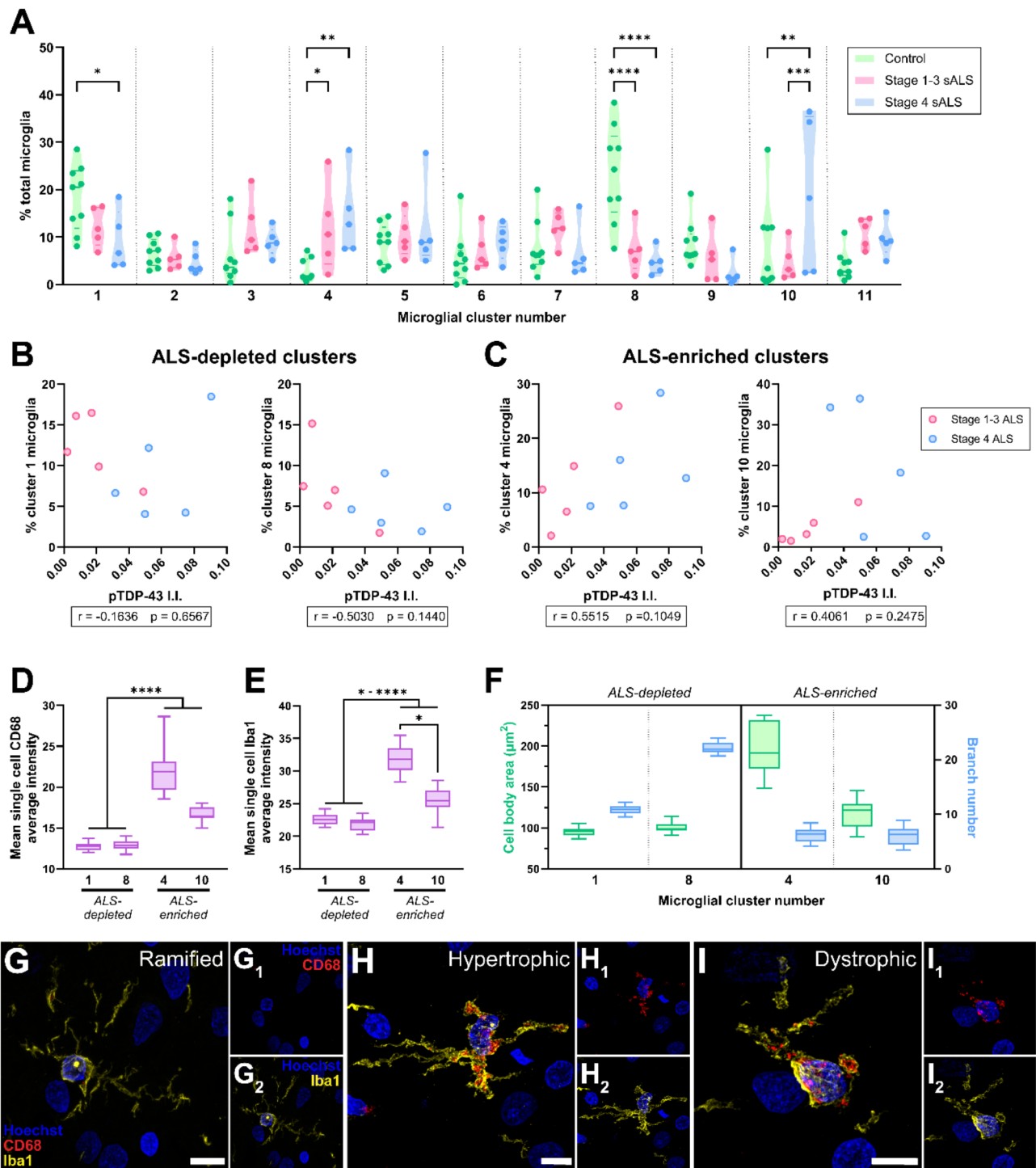


Fig. 3 (See legend on next page.)

(See figure on previous page.)

Fig. 3 Microglial clusters enriched in human ALS are characterised by high cell body area, low branch number, and high Iba1 and CD68 levels. Louvain clustering was carried out using the single-cell average intensities of CD68, HLA-DR, and Iba1, and morphological measures (cell body area, process number, outgrowth, and branch number) from a randomly subsampled 7,340 microglia per case group (22,020 cells total), resulting in 11 unique clusters (arbitrarily numbered) (**A**). The percentage of microglia in each cluster was compared between control, stage 1–3 ALS, and stage 4 ALS cases using a 2-way ANOVA with Tukey's multiple comparisons test; data presented as truncated violin plots with median and quartiles shown; control $n=10$, stage 1–3 ALS $n=5$, and stage 4 ALS $n=5$. For clusters depleted (1 and 8; **B**) and enriched (4 and 10; **C**) in ALS cases, the percentage of microglia in each cluster was correlated with pTDP-43 integrated intensity (I.I.) using Spearman's correlation; each correlation was carried out using a total $n=10$ cases, with stage 1–3 ALS and stage 4 ALS cases colour-coded and r and p values presented for each correlation. The mean single-cell CD68 and Iba1 average intensity was compared between clusters using a Kruskal-Wallis test with Dunn's multiple comparisons test (**D** and **E**); data presented for ALS-depleted and ALS-enriched clusters as a box and whisker graph, with minimum, maximum, and median shown ($n=20$). The mean cell body area and single-cell branch number were determined for all clusters (**F**); data presented for ALS-depleted and ALS-enriched clusters as a box and whisker graph, with minimum, maximum, and median shown ($n=20$). Significance of differences between groups: $*p \leq 0.05$, $**p \leq 0.01$, $***p \leq 0.001$, $****p \leq 0.0001$. Confocal microscopy was used to visualise ramified (**G**), hypertrophic (**H**), and dystrophic microglial morphologies (**I**); example images from stage 4 ALS case, MN29, are shown; scale bars = 10 μm

outgrowth and branch number, suggesting microglia become less hypertrophic and more dystrophic (Fig. 4H–K). These data are summarised in Fig. 4L.

Together these data suggest microglial changes occurred in parallel with neuronal pTDP-43 accumulation; at disease-onset, microglia increased Iba1 expression and changed towards a hypertrophic morphology, at early-disease stage, microglia increased CD68 expression and became hypertrophic, and at late-stage disease, microglia became dystrophic.

Discussion

In this study, we used fluorescent immunohistochemistry and single cell analysis pipelines to identify changes in microglial immunophenotypes and morphologies relative to pTDP-43 aggregation in the ALS motor cortex. Microglial subtypes enriched in human ALS were defined by high CD68 and Iba1 levels and hypertrophic and dystrophic morphologies. Indeed, similar microglial changes were identified in the rNLS mouse model of ALS following the onset of pTDP-43 aggregation. Overall, this study provides an examination of microglial immunophenotype and morphological changes in human ALS following pTDP-43 aggregation.

The increases in microglial CD68 and Iba1 in the ALS motor cortex significantly correlated with neuronal pTDP-43 pathology load (Fig. 1). The identified increase in CD68 corroborates our previous work where we identified a robust increase in CD68^{high} microglia in the human ALS motor cortex that correlated with pTDP-43 pathology load [39]. Because CD68 is classically considered a marker of phagocytic microglia, in the context of ALS this increase in microglial CD68 expression is hypothesised to be a reaction to the phagocytosis of pTDP-43 aggregates [20, 73–76]. The tissue-wide increase in Iba1 identified in this study also corroborates our previous work [39]. Iba1 is a cytoskeletal-associated calcium binding protein involved in membrane ruffling and phagocytosis [77–80]. Previous studies have described increases in Iba1 expression by hypertrophic, reactive microglia in the normal and *SOD1* ALS brain

[15, 17, 18, 21]. Indeed, both CD68 and Iba1 expression correlated with tissue-wide microglial morphology measures suggesting both markers are up-regulated by hypertrophic, reactive microglia (Fig. 2).

We subsequently carried out single cell analyses to better elucidate the relationship between CD68 and Iba1 expression levels and microglial morphologies. We identified CD68^{high} Iba1^{high} microglial subtypes with hypertrophic and dystrophic morphologies enriched in the human ALS motor cortex (Fig. 3). Hypertrophic microglia are considered classically reactive, with an enlarged cell body to increase metabolic activity and shortened processes to explore their immediate surroundings [50]. Dystrophic microglia show evidence of cytoplasmic fragmentation, similar to that seen in apoptotic cells, and are considered to be diseased or dysfunctional microglia [44, 50]. We therefore postulate that, in the human ALS brain, microglia change their morphologies at different points in response to pTDP-43: first, microglia increase Iba1 expression and become hypertrophic to increase metabolic activity and phagocytose pTDP-43, resulting in increased CD68 expression. Later, microglia become 'exhausted' from chronic reactions to ALS-associated pathology and degeneration, resulting in dysfunction and a dystrophic morphology. Our previous study identified high expression of the dysfunction marker, L-ferritin, in ALS-enriched clusters [39] and the specific expression of L-ferritin by dystrophic microglia in the human brain [42] validates the presence of microglial dysfunction in ALS.

Arguing against pTDP-43 pathology driving microglial immunophenotype and morphology changes in the ALS brain was the lack of significant correlations between the abundances of CD68^{high} Iba1^{high} hypertrophic and dystrophic microglial subtypes and pTDP-43 load in this study (Fig. 3C). However, this could be because large end-stage TDP-43 inclusions are unlikely to be the 'toxic species' in ALS, and the analysis pipeline used to measure pTDP-43 pathology load will not detect the other aggregation pathway species that are likely toxic; misfolded monomers and oligomers [38]. Indeed, significant

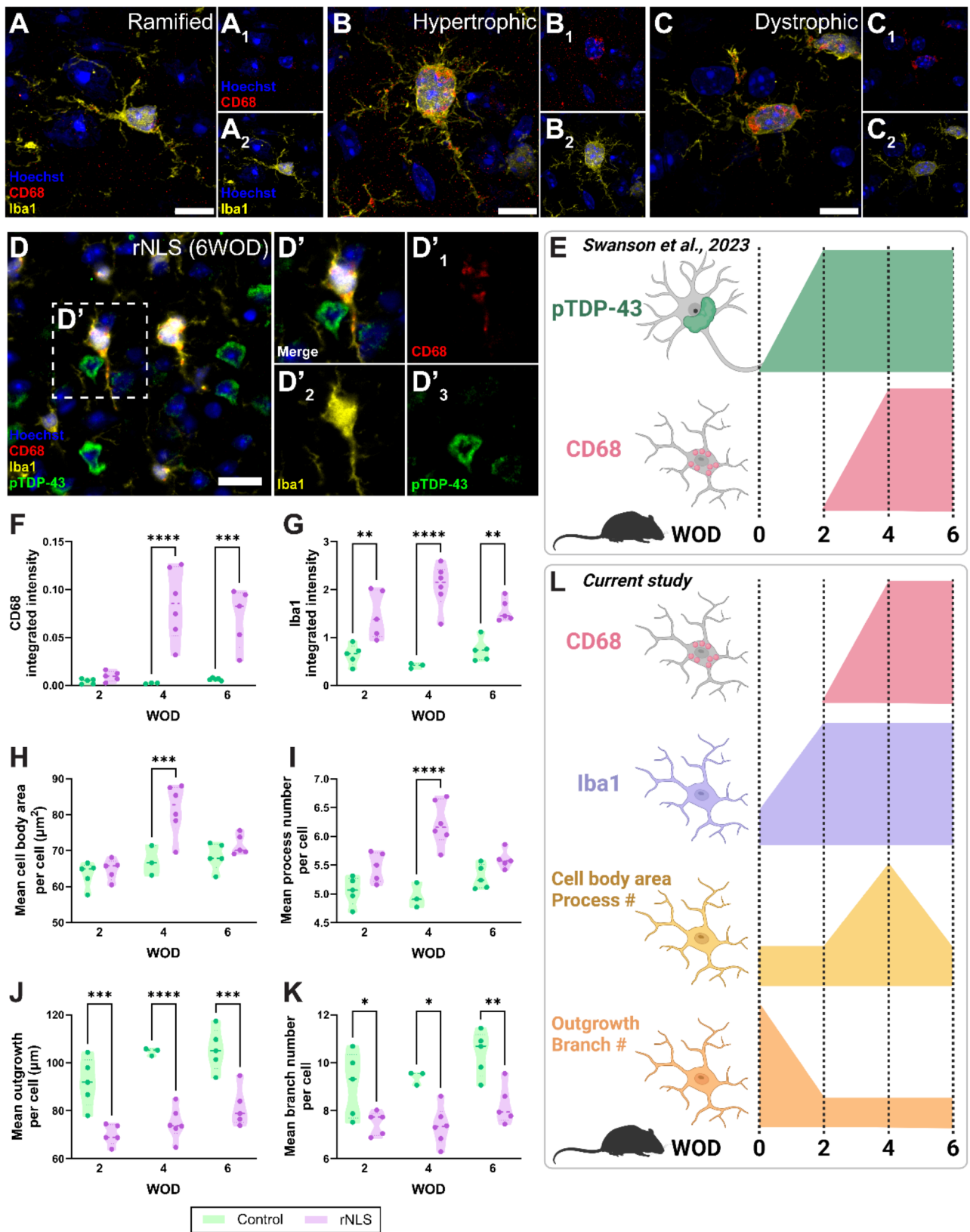


Fig. 4 (See legend on next page.)

(See figure on previous page.)

Fig. 4 Microglial Iba1 and morphological changes occur parallel to pTDP-43 aggregation and prior to CD68 changes in the TDP-43-driven rNLS mouse model of ALS. Immunohistochemical labelling of Iba1 and CD68 was carried out on motor cortex tissue from bigenic NEFH-tTA/tetO-hTDP-43 Δ NLS (rNLS) and single transgenic tetO-hTDP-43 Δ NLS (control) mice at 2, 4, and 6 weeks off DOX (WOD). Confocal microscopy was used to visualise ramified (A), hypertrophic (B), and dystrophic microglial morphologies; example images from rNLS at 6 WOD are shown; Scale bars = 10 μ m. Images previously analysed in Swanson et al., (2023) were reanalysed to investigate temporal changes in microglial morphology measures relative to pTDP-43 aggregation; an example immunohistochemical image of CD68 (red), and Iba1 (yellow), pTDP-43 (green) and a Hoechst nuclear counterstain (blue) labelling from a rNLS mouse at 6 WOD is shown (D); scalebar=20 μ m. Summary of Swanson et al., (2023) findings is shown in E; created with BioRender.com. Total microglia were identified by creating separate binary masks from CD68 and Iba1 images which were then combined to create a microglial master mask. The integrated intensities of CD68 (F) and Iba1 (G) were measured within this master mask and compared between control and rNLS mice at 2, 4, and 6 WOD. Microglial cell bodies and processes were identified using Iba1 immunoreactivity and used to quantify morphology measures per cell: cell body area (H), process number (I), outgrowth (J), and branch number (K). Single-cell measures were averaged across all microglia in each case to give a mean measure per cell which was compared between control and rNLS mice at 2, 4, and 6 WOD. Data presented as truncated violin plots with median and quartiles shown; control $n=3-5$, rNLS $n=4-6$. Each intensity and morphology measure was compared between case groups at each WOD timepoint with 2-way ANOVA with Tukey's multiple comparisons test. Significance of differences between case groups: * $p \leq 0.05$, ** $p \leq 0.01$, *** $p \leq 0.001$, **** $p \leq 0.0001$. Summary of current study's findings is shown in L; created with BioRender.com

changes were identified in microglial immunophenotypes and morphologies even in stage 1–3 cases where pTDP-43 pathology was highly variable and not significantly different overall from control, suggesting that earlier TDP-43 aggregation pathway species are directly or indirectly driving microglial changes.

While the comparison of features between stage 1–3 and stage 4 ALS cases classified on pTDP-43 load provides some insight to compare disease at different stages of progression, we were unable to assess temporal changes with certainty. To overcome this limitation, we utilised brain tissue from the rNLS TDP-43 mouse model of ALS (NEFH-tTA/tetO-hTDP-43 Δ NLS); the removal of dietary DOX induces the cytoplasmic accumulation of TDP-43 in neurons, causing motor neuron death in the spinal cord and motor cortex and associated motor phenotypes [62]. We assessed microglial immunophenotype and morphology changes at 2, 4, and 6 WOD, equivalent to disease onset, early disease, and late disease stages, respectively (Fig. 4). In our previous study, we identified a significant increase in pTDP-43 aggregate load by 2 WOD, with microglial CD68 levels increasing at 4 WOD [39]. In this study, we identified that microglia increase Iba1 expression and change to a hypertrophic morphology by 2 WOD (in parallel with pTDP-43 aggregation), microglia then increase CD68 expression at 4 WOD, and change to a dystrophic morphology at 6 WOD. These data support our hypotheses based on human tissue findings: that microglia change morphologies to aid in their phagocytosis of pTDP-43 but chronic reactivity results in dysfunction and dystrophy.

We have demonstrated microglial changes correlating with pTDP-43 pathology in ALS, but it is important to consider the plethora of stimuli in the brain to which microglia respond, including other cell types [81]. For example, a recent study demonstrated microglia respond to motor cortical hyperactivity, a clinical feature of ALS [82], through significant immunophenotype and morphological changes [41]. A unique rod-shaped microglial subpopulation interacting with neuronal dendrites and

excitatory synapses was identified and suggested to have a neuroprotective role [43]. Interestingly, mislocalisation of TDP-43 from the nucleus to the cytoplasm (an early step in the TDP-43 aggregation pathway) has been shown to cause cortical hyperexcitability in the rNLS mouse model [83]. There is therefore a link between microglial reactivity, neuronal hyperexcitability, and pTDP-43 pathology. As with microglia, astrocytes show significant reactivity in ALS, with significant debate as to whether astrocytes play a neuroprotective or neurotoxic role in ALS pathogenesis (for review see [84]). Interestingly, the role of astrocyte-microglia crosstalk in ALS pathogenesis has been discussed, with microglial disease-phenotypes hypothesised to drive astrocytic changes and vice versa [85]. Our previous study reported a significant increase in astrocyte area coverage in the human ALS motor cortex which did not correlate with pTDP-43 pathology load or any microglial protein measure [39]. Overall, disease-associated interactions between microglia, neurons, and astrocytes remain unclear, but should be considered in the future when assessing microglial changes in ALS.

This study used a refined immunofluorescent panel of three commonly used microglial functional markers (HLA-DR, CD68, and Iba1) with single-cell analysis pipelines to assess microglial immunophenotype and morphology changes in ALS. However, neither these markers nor morphologies fully capture microglial heterogeneity of the human brain in health or disease. Iba1 and HLA-DR were not expressed in all microglial states in the normal and Alzheimer's disease brain [42, 86–88]. In the context of ALS, our previous study identified a tissue-wide increase in Iba1 levels, but Louvain clustering of single cell immunophenotypes did not reveal a higher expression of Iba1 in microglial states enriched in the ALS motor cortex [39]. However, in the current study where microglial morphologies were quantified and included as metrics in single-cell clustering, Iba1 was expressed more highly in ALS-enriched microglial states; likely a reflection of the functional link between Iba1 and morphology changes. Therefore, the more

aspects of microglial phenotypes accounted for by analysis, the greater the depth of data, and the more specific disease-associated states identified. We have demonstrated that multiplexed immunohistochemistry and image analysis approaches can be integrated to identify microglial heterogeneity and subtle microglial state changes in disease.

The primary limitation of this study is that we are predicting changes in microglial function in ALS based on immunophenotype and morphology changes in post-mortem tissues. In vitro models like induced pluripotent stem cell derived microglia-like cells (iPSC-microglia) can recapitulate in vivo microglial phenotypes and provide an opportunity for future investigations of the functional implications of immunophenotype and morphology changes [89–91]. In this study, the analysis of microglial immunophenotypes and morphology in end-stage ALS patient tissue and a mouse model of ALS allows us to create a strong hypothesis of microglial functional changes in the ALS brain. However, one of the dominating narratives on microglia in the ALS field is the idea of microglia being neuroprotective in early-stage disease and neurotoxic in late-stage disease. This hypothesis was first proposed as microglia isolated from early-stage *G93A SOD1* mice were neurotrophic when co-cultured with neurons, whereas microglia from late-stage *G93A SOD1* mice were neurotoxic [31]. As a neurotoxic microglial phenotype can be induced by native and mutant forms of TDP-43 in vitro [32], it is hypothesized that this neurotrophic-to-neurotoxic change also happens in the 97% of ALS cases with TDP-43 pathology. Indeed, a recent study by Xie and colleagues demonstrated a neuroprotective microglial phenotype in rNLS mice and sporadic human ALS brains [41]; rod microglia emerge in at early-stage disease and have a neuroprotective transcriptomic signature. However, as Xie and colleagues do not describe the presence of hypertrophic and dystrophic microglial morphologies characteristic of microglia in human diseased brains, it is difficult to draw similarities to their study and our current study. The data presented in this study cannot confirm nor negate the neurotrophic-to-neurotoxic hypothesis; further functional studies investigating the effects of these immunophenotype and morphological changes are needed. However, we validate the presence of dysfunctional microglia in the end-stage disease ALS brain reflecting a potential loss of trophic support from microglia in late-stage disease. Studies either reversing dysfunctional microglial states, for example by direct genetic manipulation of key genes, or transplanting homeostatic microglia are needed to identify whether the reversal of microglial dysfunction and enhanced microglial trophic support could slow ALS pathogenesis.

Conclusions

Overall, the evidence presented in this study demonstrates that microglia change their morphologies prior to immunophenotype changes. We hypothesise these morphological changes aid the disease-related reactivity to neuronal pTDP-43 aggregates, which triggers immunophenotype changes; first, to a phagocytic state then to a dysfunctional one.

Abbreviations

ALS	Amyotrophic lateral sclerosis
HLA-DR	Human leukocyte antigen – DR isotype
HuBB	Neurological Foundation Human Brain Bank
Iba1	Ionised calcium binding adaptor molecule 1
KNN	K-nearest neighbours
pTDP-43	Phosphorylated TAR DNA-binding protein 43
rNLS	Bigenic <i>NEFH-tTA/tetO-hTDP-43ΔNLS</i> mice
ROI	Region of interest
TDP-43	TAR DNA-binding protein 43
WOD	Weeks off doxycycline

Supplementary Information

The online version contains supplementary material available at <https://doi.org/10.1186/s40478-025-01941-0>.

Supplementary Material 1

Acknowledgements

This publication is dedicated to the incredible patients and families who contribute to our research. We thank Marika Eszes at the Centre for Brain Research, University of Auckland, New Zealand, and the Neurological Foundation of New Zealand for their ongoing financial support of the Human Brain Bank. The imaging data reported in this paper were obtained at the Biomedical Imaging Research Unit, operated by the Faculty of Medical and Health Sciences' Technical Services at the University of Auckland.

Author contributions

MEVS, AKW, and ELS conceptualized the study. RLMF and MAC collected and processed the human tissue. CT carried out pathological assessment of all cases. MEVS and MM carried out the experimental procedures. MEVS and ELS developed the custom image analysis pipelines. MEVS and MM carried out quantification. Data analysis and interpretation were carried out by MEVS, MM, and ELS. Manuscript was prepared by MEVS and ELS. All authors read and approved of the final manuscript.

Funding

MEVS was supported by the Neurological Foundation of New Zealand (First Fellowship, Philip Wrightson Fellowship, and Small Project Grant). AKW was supported by FightMND (Bill Guest Mid-Career Research Fellowship), the Ross Maclean Fellowship, and the Brazil Family Program for Neurology. ELS was supported by Rutherford Discovery Fellowship funding from the Royal Society of New Zealand [15-UOA-003]. No funding body played any role in the design of the study, nor in the collection, analysis, or interpretation of data nor in writing the manuscript.

Data availability

No datasets were generated or analysed during the current study.

Declarations

Ethics approval and consent to participate

All human brain tissue was donated to the Neurological Foundation Human Brain Bank following donor and donor family consent, and its use in this study was approved by the University of Auckland Human Participants Ethics committee (protocol number 011654). Animal ethics approval was obtained from The University of Queensland (#QBI/131/18), and experiments were

conducted in accordance with the Australian code of practice for the care and use of animals for scientific purposes.

Consent for publication

Not applicable.

Competing interests

The authors declare no competing interests.

Author details

¹School of Biological Sciences, University of Auckland, Auckland, New Zealand

²Centre for Brain Research, University of Auckland, Auckland, New Zealand

³Department of Anatomical Pathology, Pathology and Laboratory Medicine, Auckland City Hospital, Auckland, New Zealand

⁴Department of Anatomy and Medical Imaging, University of Auckland, Auckland, New Zealand

⁵Clem Jones Centre for Ageing Dementia Research, Queensland Brain Institute, The University of Queensland, Brisbane, Australia

Received: 26 November 2024 / Accepted: 29 January 2025

Published online: 21 February 2025

References

- Aderem A, Underhill DM (2002) Mechanisms of Phagocytosis in macrophages. *Annu Rev Immunol* 17:593–623
- Gibbons HM, Smith AM, Teoh HH, Bergin PM, Mee EW, Faull RLM et al (2011) Valproic acid induces microglial dysfunction, not apoptosis, in human glial cultures. *Neurobiol Dis* 41:96–103
- Rogers J, Strohmeyer R, Kovelowski CJ, Li R (2002) Microglia and inflammatory mechanisms in the clearance of amyloid beta peptide. *Glia* 40:260–269
- Simard AR, Soulet D, Gowing G, Julien J-P, Rivest S (2006) Bone marrow-derived microglia play a critical role in restricting senile plaque formation in Alzheimer's disease. *Neuron* 49:489–502
- Chhor V, Le Charpentier T, Lebon S, Oré M-V, Celador IL, Jossierand J et al (2013) Characterization of phenotype markers and neuronotoxic potential of polarised primary microglia in vitro. *Brain Behav Immun* 32:70–85
- Melief J, Koning N, Van De Schuurman KG, Smolders J, Hoek RM et al (2012) Phenotyping primary human microglia: tight regulation of LPS responsiveness. *Glia* 60:1506–1517
- Peferoen LAN, Vogel DYS, Ummenthum K, Breur M, Heijnen PDAM, Gerritsen WH et al (2015) Activation status of human microglia is dependent on lesion formation stage and remyelination in multiple sclerosis. *J Neuropathol Exp Neurol* 74:48–63
- Dijkstra IM, van der Hulshof S, Boddeke HWGM, Biber K (2014) Cutting Edge: activity of human adult microglia in response to CC Chemokine Ligand 21. *J Immunol* 172:2744–2747
- El Khoury J, Hickman SE, Thomas CA, Cao L, Silverstein SC, Loike JD (1996) Scavenger receptor-mediated adhesion of microglia to beta-amyloid fibrils. *Nature* 382:716–719
- Lively S, Schlichter LC (2013) The microglial activation state regulates migration and roles of matrix-dissolving enzymes for invasion. *J Neuroinflammation* 10:75
- Yan SD, Chen X, Fu J, Chen M, Zhu H, Roher A et al (1996) RAGE and amyloid-beta peptide neurotoxicity in Alzheimer's disease. *Nature* 382:685–691
- McGeer PL, Itagaki S, Tago H, McGeer EG (1987) Reactive microglia in patients with senile dementia of the Alzheimer type are positive for the histocompatibility glycoprotein HLA-DR. *Neurosci Lett* 79:195–200
- McGeer PL, Itagaki S, McGeer EG (1988) Expression of the histocompatibility glycoprotein HLA-DR in neurological disease. *Acta Neuropathol* 76:550–557
- Graber DJ, Hickey WF, Harris BT (2010) Progressive changes in microglia and macrophages in spinal cord and peripheral nerve in the transgenic rat model of amyotrophic lateral sclerosis. *J Neuroinflammation* 7:1–12
- Stamenković S, Dučić T, Stamenković V, Kranz A, Andjus PR (2017) Imaging of glial cell morphology, SOD1 distribution and elemental composition in the brainstem and hippocampus of the ALS hSOD1G93A rat. *Neuroscience* 357:37–55
- Sanagi T, Yuasa S, Nakamura Y, Suzuki E, Aoki M, Warita H et al (2010) Appearance of phagocytic microglia adjacent to motoneurons in spinal cord tissue from a presymptomatic transgenic rat model of amyotrophic lateral sclerosis. *J Neurosci Res* 88:2736–2746
- Gerber YN, Sabourin JC, Rabano M, Vivanco MdM, Perrin FE (2012) Early functional deficit and microglial disturbances in a mouse model of amyotrophic lateral sclerosis. *PLoS ONE*;7
- Ohgomori T, Yamada J, Takeuchi H, Kadomatsu K, Jinno S (2016) Comparative morphometric analysis of microglia in the spinal cord of SOD1G93A transgenic mouse model of amyotrophic lateral sclerosis. *Eur J Neurosci* 43:1340–1351
- Schludi MH, Becker L, Garrett L, Gendron TF, Zhou Q, Schreiber F et al (2017) Spinal poly-GA inclusions in a C9orf72 mouse model trigger motor deficits and inflammation without neuron loss. *Acta Neuropathol* 134:241–254
- Spiller KJ, Restrepo CR, Khan T, Dominique MA, Fang TC, Canter RG et al (2018) Microglia-mediated recovery from ALS-relevant motor neuron degeneration in a mouse model of TDP-43 proteinopathy. *Nat Neurosci* 21:329–340
- Jara JH, Genç B, Stanford MJ, Pytel P, Roos RP, Weintraub S et al (2017) Evidence for an early innate immune response in the motor cortex of ALS. *J Neuroinflammation* 14:1–20
- Chiu IM, Morimoto ETA, Goodarzi H, Liao JT, O'Keefe S, Phatnani HP et al (2013) A neurodegeneration-specific gene-expression signature of acutely isolated microglia from an amyotrophic lateral sclerosis mouse model. *Cell Rep* 4:385–401
- Funikov SY, Rezvykh AP, Mazin PV, Morozov AV, Maltsev AV, Chicheva MM et al (2018) FUS(1-359) transgenic mice as a model of ALS: pathophysiological and molecular aspects of the proteinopathy. *Neurogenetics* 19:189–204
- Beers DR, Zhao W, Liao B, Kano O, Wang J, Huang A et al (2011) Neuroinflammation modulates distinct regional and temporal clinical responses in ALS mice. *Brain Behav Immun* 25:1025–1035
- Mitchell JC, McGoldrick P, Vance C, Hortobagyi T, Sreedharan J, Rogelj B et al (2013) Overexpression of human wild-type FUS causes progressive motor neuron degeneration in an age- and dose-dependent fashion. *Acta Neuropathol* 125:273–288
- Kwan JY, Jeong SY, van Gelderen P, Deng HX, Quezado MM, Danielian LE et al (2012) Iron accumulation in deep cortical layers accounts for MRI signal abnormalities in ALS: correlating 7 tesla MRI and pathology. *PLoS ONE*;7
- Nolan M, Scott C, Gamarallage MP, Lunn D, Carpenter K, McDonough E et al (2020) Quantitative patterns of motor cortex proteinopathy across ALS genotypes. *Acta Neuropathol Commun* 8:98
- Liu W, Venugopal S, Majid S, Ahn IS, Diamante G, Hong J et al (2020) Single-cell RNA-seq analysis of the brainstem of mutant SOD1 mice reveals perturbed cell types and pathways of amyotrophic lateral sclerosis. *Neurobiol Dis* 141:104877
- Dachet F, Liu J, Ravits J, Song F (2019) Predicting disease specific spinal motor neurons and glia in sporadic ALS. *Neurobiol Dis* 130:104523
- Dols-Icardo O, Montal V, Sirisi S, López-Pernas G, Cervera-Carles L, Querol-Vilaseca M et al (2020) Motor cortex transcriptome reveals microglial key events in amyotrophic lateral sclerosis. *Neurol - Neuroimmunol Neuroinflammation* 7:e829
- Liao B, Zhao W, Beers DR, Henkel JS, Appel SH (2012) Transformation from a neuroprotective to a neurotoxic microglial phenotype in a mouse model of ALS. *Exp Neurol* 237:147–152
- Zhao W, Beers DR, Bell S, Wang J, Wen S, Baloh RH et al (2015) TDP-43 activates microglia through NF-κB and NLRP3 inflammasome. *Exp Neurol* 273:24–35
- Humphrey J, Venkatesh S, Hasan R, Herb JT, de Paiva Lopes K, Küçükali F et al (2023) Integrative transcriptomic analysis of the amyotrophic lateral sclerosis spinal cord implicates glial activation and suggests new risk genes. *Nat Neurosci* 26:150–162
- Mandrioli J, Faglioni P, Nichelli P, Sola P (2006) Amyotrophic lateral sclerosis: prognostic indicators of survival. *Amyotroph Lateral Scler* 7:217–226
- Scotter EL, Chen H-J, Shaw CE (2015) TDP-43 Proteinopathy and ALS: insights into Disease mechanisms and therapeutic targets. *Neurotherapeutics* 12:352–363
- Al-Chalabi A, Calvo A, Chio A, Colville S, Ellis CM, Hardiman O et al (2014) Analysis of amyotrophic lateral sclerosis as a multistep process: a population-based modelling study. *Lancet Neurol* 13:1108–1113
- Neumann M, Sampathu DM, Kwong LK, Truax AC, Micsenyi MC, Chou TT et al (2006) Ubiquitinated TDP-43 in frontotemporal lobar degeneration and amyotrophic lateral sclerosis. *Science* 314:130–133
- Keating SS, San Gil R, Swanson MEV, Scotter EL, Walker AK (2022) TDP-43 pathology: from noxious assembly to therapeutic removal. *Prog Neurobiol* 211:102229

39. Swanson MEV, Mrkela M, Murray HC, Cao MC, Turner C, Curtis MA et al (2023) Microglial CD68 and L-ferritin upregulation in response to phosphorylated-TDP-43 pathology in the amyotrophic lateral sclerosis brain. *Acta Neuropathol Commun* 11:69
40. Hunter M, Spiller KJ, Dominique MA, Xu H, Hunter FW, Fang TC et al (2021) Microglial transcriptome analysis in the rNLS8 mouse model of TDP-43 proteinopathy reveals discrete expression profiles associated with neurodegenerative progression and recovery. *Acta Neuropathol Commun* 9:1–19
41. Xie M, Alessandra MS, Praveen PN, Umpierre A, Liang Y, Wang N et al (2024) Rod-shaped microglia interact with neuronal dendrites to regulate cortical excitability in TDP-43 related neurodegeneration. *bioRxiv* (Preprint) 1–21. <https://doi.org/10.1101/2024.06.30.601396>
42. Swanson MEV, Murray HC, Ryan B, Faull RLM, Draganow M, Curtis MA (2020) Quantitative immunohistochemical analysis of myeloid cell marker expression in human cortex captures microglia heterogeneity with anatomical context. *Sci Rep* 10:11693
43. Bachstetter AD, Ighodaro ET, Hassoun Y, Aldeiri D, Neltner JH, Patel E et al (2017) Rod-shaped microglia morphology is associated with aging in 2 human autopsy series. *Neurobiol Aging* 52:98–105
44. Bachstetter AD, Van Eldik LJ, Schmitt FA, Neltner JH, Ighodaro ET, Webster SJ et al (2015) Disease-related microglia heterogeneity in the hippocampus of Alzheimer's disease, dementia with Lewy bodies, and hippocampal sclerosis of aging. *Acta Neuropathol Commun* 3:1–16
45. Streit WJ, Khoshbouei H, Bechmann I (2020) Dystrophic microglia in late-onset Alzheimer's disease. *Glia* 68:845–854
46. Lopes KO, Sparks DL, Streit WJ (2008) Microglial dystrophy in the aged and Alzheimer's disease brain is associated with ferritin immunoreactivity. *Glia* 56:1048–1060
47. Streit WJ, Walter SA, Pennell NA (1999) Reactive microgliosis. *Prog Neurobiol* 57:563–581
48. Streit WJ, Braak H, Xue QS, Bechmann I (2009) Dystrophic (senescent) rather than activated microglial cells are associated with tau pathology and likely precede neurodegeneration in Alzheimer's disease. *Acta Neuropathol* 118:475–485
49. Streit WJ, Miller KR, Lopes KO, Njie E (2008) Microglial degeneration in the aging brain - bad news for neurons? *Front Biosci* 13:3423–3438
50. Streit WJ, Xue Q-S, Tischer J, Bechmann I (2014) Microglial pathology. *Acta Neuropathol Commun* 2:142
51. Paolicelli RC, Sierra A, Stevens B, Tremblay ME, Aguzzi A, Ajami B et al (2022) Microglia states and nomenclature: a field at its crossroads. *Neuron* 110:3458–3483
52. Stence N, Waite M, Dailey ME (2001) Dynamics of microglial activation: a confocal time-lapse analysis in hippocampal slices. *Glia* 33:256–266
53. Sierra A, Encinas JM, Deudero JJPP, Chancey JH, Enikolopov G, Overstreet-Wadiche LS et al (2010) Microglia shape adult hippocampal neurogenesis through apoptosis-coupled phagocytosis. *Cell Stem Cell* 7:483–495
54. Sierra A, Abiega O, Shahraz A, Neumann H (2013) Janus-faced microglia: beneficial and detrimental consequences of microglial phagocytosis. *Front Cell Neurosci* 7:1–22
55. Peri F, Nüsslein-Volhard C (2008) Live imaging of neuronal degradation by Microglia reveals a role for v0-ATPase a1 in Phagosomal Fusion in vivo. *Cell* 133:916–927
56. Streit WJ, Xue QS (2009) Life and death of microglia. *J Neuroimmune Pharmacol* 4:371–379
57. Taylor SE, Morganti-Kossmann C, Lifshitz J, Ziebell JM (2014) Rod microglia: a morphological definition. *PLoS ONE* 9:e97096
58. Aronica E, Baas F, Iyer A, ten Asbroek ALMA, Morello G, Cavallaro S (2015) Molecular classification of amyotrophic lateral sclerosis by unsupervised clustering of gene expression in motor cortex. *Neurobiol Dis* 74:359–376
59. Keren-Shaul H, Spinrad A, Weiner A, Matcovitch-Natan O, Dvir-Szternfeld R, Ulland TK et al (2017) A Unique Microglia Type Associated with Restricting Development of Alzheimer's Disease. *Cell* 169:1276–1290e17
60. Maniatis S, Vickovic S, Braine C, Kang K, Mollbrink A, Fagegaltier D et al (2019) Spatiotemporal dynamics of molecular pathology in amyotrophic lateral sclerosis. *Sci* (1979) 364:89–93
61. Zhou Q, Mareljic N, Michaelsen M, Parhizkar S, Heindl S, Nuscher B et al (2020) Active poly-GA vaccination prevents microglia activation and motor deficits in a C9orf72 mouse model. *EMBO Mol Med* 12:1–13
62. Walker AK, Spiller KJ, Ge G, Zheng A, Xu Y, Zhou M et al (2015) Functional recovery in new mouse models of ALS/FTLD after clearance of pathological cytoplasmic TDP-43. *Acta Neuropathol* 130:643–660
63. Bretschneider J, Del Tredici K, Toledo JB, Robinson JL, Irwin DJ, Grossman M et al (2013) Stages of pTDP-43 pathology in amyotrophic lateral sclerosis. *Ann Neurol* 74:20–38
64. Waldvogel HJ, Curtis MA, Baer K, Rees MI, Faull RLM (2007) Immunohistochemical staining of post-mortem adult human brain sections. *Nat Protoc* 1:2719–2732
65. Wright AL, Della Gatta PA, Le S, Berning BA, Mehta P, Jacobs KR et al (2021) Riluzole does not ameliorate disease caused by cytoplasmic TDP-43 in a mouse model of amyotrophic lateral sclerosis. *Eur J Neurosci* 54:6237–6255
66. Murray HC, Dieriks BV, Swanson MEV, Anekal PV, Turner C, Faull RLM et al (2020) The unfolded protein response is activated in the olfactory system in Alzheimer's disease. *Acta Neuropathol Commun* 8:109
67. Dieriks BV, Dean JM, Aronica E, Waldvogel HJ, Faull RLM, Curtis MA (2018) Differential fatty acid-binding protein expression in persistent radial glia in the human and sheep subventricular zone. *Dev Neurosci* 40:145–161
68. Waters S, Swanson MEV, Dieriks BV, Zhang YB, Grimsey NL, Murray HC et al (2021) Blood-spinal cord barrier leakage is independent of motor neuron pathology in ALS. *Acta Neuropathol Commun* 9:1–17
69. Woolf Z, Swanson MEV, Smyth LC, Mee EW, Schweder P, Heppner P et al (2021) Single-cell image analysis reveals a protective role for microglia in glioblastoma. *Neurooncol Adv*;3
70. Beygelzimer A, Kakadet S, Langford J, Arya S, Mount D, Li S (2019) FNN: Fast Nearest Neighbor Search Algorithms and Applications
71. Csardi G, Nepusz T The igraph software package for complex network research. *InterJournal [Internet]*. 2006;Complex sy. Available from: <https://igraph.org>
72. Singh-Bains MK, Linke V, Austria MDR, Tan AYS, Scotter EL, Mehrabi NF et al (2019) Altered microglia and neurovasculature in the Alzheimer's disease cerebellum. *Neurobiol Dis* 132:104589
73. Zotova E, Bharambe V, Cheaveau M, Morgan W, Holmes C, Harris S et al (2013) Inflammatory components in human Alzheimer's disease and after active amyloid- β 42 immunization. *Brain* 136:2677–2696
74. Holness CL, Simmons DL (1993) Molecular cloning of CD68, a human macrophage marker related to lysosomal glycoproteins. *Blood* 81:1607–1613
75. Xie M, Liu YU, Zhao S, Zhang L, Bosco DB, Pang YP et al (2022) TREM2 interacts with TDP-43 and mediates microglial neuroprotection against TDP-43-related neurodegeneration. *Nat Neurosci* 25:26–38
76. Svahn AJ, Don EK, Badrock AP, Cole NJ, Graeber MB, Yerbury JJ et al (2018) Nucleo-cytoplasmic transport of TDP-43 studied in real time: impaired microglia function leads to axonal spreading of TDP-43 in degenerating motor neurons. *Acta Neuropathol* 136:445–459
77. Ohsawa K, Imai Y, Sasaki Y, Kohsaka S (2004) Microglia/macrophage-specific protein Iba1 binds to fimbriin and enhances its actin-bundling activity. *J Neurochem* 88:844–856
78. Sasaki Y, Ohsawa K, Kanazawa H, Kohsaka S, Imai Y (2001) Iba1 is an actin-cross-linking protein in macrophages/microglia. *Biochem Biophys Res Commun* 286:292–297
79. Ohsawa K, Imai Y, Kanazawa H, Sasaki Y, Kohsaka S (2000) Involvement of Iba1 in membrane ruffling and phagocytosis of macrophages/microglia. *J Cell Sci* 113:3073–3084
80. Imai Y, Ibata I, Ito D, Ohsawa K, Kohsaka S (1996) A novel gene iba1 in the major histocompatibility complex class III region encoding an EF hand protein expressed in a monocytic lineage. *Biochem Biophys Res Commun* 224:855–862
81. Murray HC, Johnson K, Sedlock A, Highet B, Dieriks BV, Anekal PV et al (2022) Lamina-specific immunohistochemical signatures in the olfactory bulb of healthy, Alzheimer's and Parkinson's disease patients. *Commun Biol* 5:1–12
82. Van den Geervasinga N, Menon P, Vucic S (2021) Utility of transcranial magnetic stimulation in studying upper motor neuron dysfunction in amyotrophic lateral sclerosis. *Brain Sci* 11
83. Dyer MS, Reale LA, Lewis KE, Walker AK, Dickson TC, Woodhouse A et al (2021) Mislocalisation of TDP-43 to the cytoplasm causes cortical hyperexcitability and reduced excitatory neurotransmission in the motor cortex. *J Neurochem* 157:1300–1315
84. You J, Youssef MMM, Santos JR, Lee J, Park J (2023) Microglia and astrocytes in amyotrophic lateral sclerosis: disease-associated states, pathological roles, and therapeutic potential. *Biol (Basel)* 12:1307. <https://doi.org/10.3390/biolog12101307>
85. Calafatti M, Coccozza G, Limatola C, Garofalo S (2023) Microglial crosstalk with astrocytes and immune cells in amyotrophic lateral sclerosis. *Front Immunol* 14:1–12

86. Swanson MEV, Scotter EL, Murray HC, Turner C, Faull RLMM, Curtis MA et al (2020) Identification of a dysfunctional microglial population in human Alzheimer's disease cortex using novel single-cell histology image analysis. *Acta Neuropathol Commun* 8:1–16
87. Hendrickx DAEE, van Eden CG, Schuurman KG, Hamann J, Huitinga I (2017) Staining of HLA-DR, Iba1 and CD68 in human microglia reveals partially overlapping expression depending on cellular morphology and pathology. *J Neuroimmunol* 309:12–22
88. Kenkhuis B, Somarakis A, Kleindouwel LRT, van Roon-Mom WMC, van der Höllt T (2022) Co-expression patterns of microglia markers Iba1, TMEM119 and P2RY12 in Alzheimer's disease. *Neurobiol Dis* 167:105684
89. Abud EM, Ramirez RN, Martinez ES, Healy LM, Nguyen CHH, Newman SA et al (2017) iPSC-Derived human microglia-like cells to Study Neurological diseases. *Neuron* 94:278–293e9
90. Hasselmann J, Blurton-Jones M (2020) Human iPSC-derived microglia: a growing toolset to study the brain's innate immune cells. *Glia* 68:721–739
91. Vahsen BF, Gray E, Candalija A, Cramb KML, Scaber J, Dafinca R et al (2022) Human iPSC co-culture model to investigate the interaction between microglia and motor neurons. *Sci Rep* 12

Publisher's note

Springer Nature remains neutral with regard to jurisdictional claims in published maps and institutional affiliations.